



Interseismic slip rate of the Garze–Yushu fault belt in the Tibetan Plateau from C-band InSAR observations between 2003 and 2010

Yang Liu^{a,b}, Caijun Xu^{a,*}, Zhenhong Li^b, Yangmao Wen^a, David Forrest^b

^a School of Geodesy and Geomatics, Wuhan University, 129 Luoyu Road, Wuhan 430079, China

^b COMET+, School of Geographical and Earth Sciences, University of Glasgow, University Avenue, Glasgow G12 8QQ, United Kingdom

Received 30 April 2011; received in revised form 15 August 2011; accepted 20 August 2011

Abstract

InSAR time series techniques can provide high-spatial resolution deformation fields across an active fault belt, even for zones with heavy vegetation coverage. An interseismic deformation map across the Garze–Yushu fault belt in the Tibetan Plateau, ~300 km by ~100 km, is derived from C-band Envisat/ASAR imagery collected between 2003 and 2010. Unlike previous research, we obtain a lookup figure which relates the slip rate with the fault locking depth, the dip angle and the rake angle. The estimated slip rate changes significantly with the locking depth and the rake angle, but relatively little with the dip angle. When considering the focal mechanism solutions of historical earthquake along the Garze–Yushu fault, the interseismic slip rate of the Garze–Yushu fault is close to a value of 6.4 mm/yr, which is between the highest (18.2 mm/yr) and the lowest (3.1 mm/yr) slip rate from GPS estimations, but slightly less than the minimum value (~7 mm/yr) from the geological estimations. The earthquake recurrence interval on the Yushu part of Garze–Yushu fault equals 272 yr, and the April 14, 2010 Mw 6.9 earthquake has not completely released the accumulated strain energy between 1738 and 2010.

© 2011 COSPAR. Published by Elsevier Ltd. All rights reserved.

Keywords: Interseismic slip rate; Garze–Yushu fault belt; InSAR; Tibetan Plateau; Recurrence interval

1. Introduction

To predict the earthquake probability along an active fault in the future, a high spatial resolution and high precision strain (rate) map is needed. GPS can measure small surface movements of a magnitude of up to sub-mm and can provide high frequency signals up to 1 Hz or greater (Bock et al., 2004; Larson et al., 2003). However, to achieve more than about 0.5-km sampling of deformation measurement requires a dramatic densification of the GPS observation stations, which is costly and therefore unlikely to happen (Wei et al., 2010). Due to its high spatial resolution (e.g., up to tens of meters for Envisat satellite and up to 1 m

for TerraSAR-X), Interferometric Synthetic Aperture Radar (InSAR) can complement this disadvantage of GPS to measure surface deformation and can be an useful tool to monitor the near-fault strain accumulation and release.

InSAR, which can obtain the large-scale, minor-magnitude position change, is a unique technique to monitor crustal deformation, especially for interseismic movements across active fault belts. When InSAR is used to measure the surface displacement, the main errors consist of the lack of accurate satellite orbits, tropospheric and ionospheric disturbances, and other random noise (Hanssen, 2001). Based on multi-temporal interferograms, InSAR time series methods can address these problems to provide a quite high-precision deformation series, even for zones with heavy vegetation coverage and small magnitude

* Corresponding author. Tel.: +86 27 68778805; fax: +86 27 68778371.
E-mail address: cjxu@sgg.whu.edu.cn (C. Xu).

deformation signal (Biggs et al., 2007; Cavalié et al., 2008; Elliott et al., 2008; Gourmelen et al., 2010; Li et al., 2009; Wang et al., 2009).

On April 14, 2010, an Mw 6.9 earthquake occurred on the Garze–Yushu fault belt, located in the center of the Tibetan Plateau (Fig. 1). The Garze–Yushu fault belt strikes northwest and runs through Zhiduo, Dangjiang, Yushu, Dengke, and Garze counties from NW to SE, with a length of about 500 km (Peng et al., 2006). Together with the Xianshuihe fault belt, the Garze–Yushu fault belt forms the northern boundary of the Sichuan–Yunnan active tectonic block and the Qiangtang active tectonic block and the southern boundary of Bayankala active tectonic block (Zhang et al., 2003). It dominates the tectonic activities and the recurrence of the characteristic earthquakes.

Previous geological studies have suggested that the Quaternary strike-slip rate of the Garze–Yushu fault belt ranges from 7 mm/yr to 14 mm/yr (Wang et al., 2008a; Wen et al., 2003; Zhou et al., 1996). Based on the faulted landform, displacement of young deposit layers and geologic chronology, Zhou et al. (1996) determined that the average slip rate of the Yushu part of the Garze–Yushu

fault belt since later quaternary is about 7 mm/yr. Wen et al. (2003) suggested the average left-lateral slip rate along the Garze–Yushu fault of about 12 mm/yr using the later Quaternary activity and recent large earthquake ruptures. Based on the distribution of stream deflections along the Garze–Yushu segment of the Xianshuihe fault, Wang et al. (2008a) proposed that the Holocene slip rate along it decreases from 10 to 14 mm/yr around Dengke (SE) to about 7 mm/yr around Dangjiang (NW). The GPS velocity field across the fault belt indicates that the decennial-scale strike-slip rate of the fault belt is around 10 mm/yr (Gan et al., 2007; Meade, 2007; Wang et al., 2008b, 2011), which is consistent with the magnitude on the millennial-scale. Using a simple dislocation model in an elastic half space (Okada, 1992) and GPS data, Gan et al. (2007) found that the average left-lateral slip rate along the Xianshuihe fault (including the Yushu segment studied in this research) as a whole is 14.4 mm/yr. Based on a three-dimensional, regional-scale elastic crustal block model and GPS data, Meade (2007) reported that the Yushu fault slip left laterally at about 10 mm/yr. Using the least squares method and GPS data, Wang et al. (2008b) employed a linked-fault-element model to invert

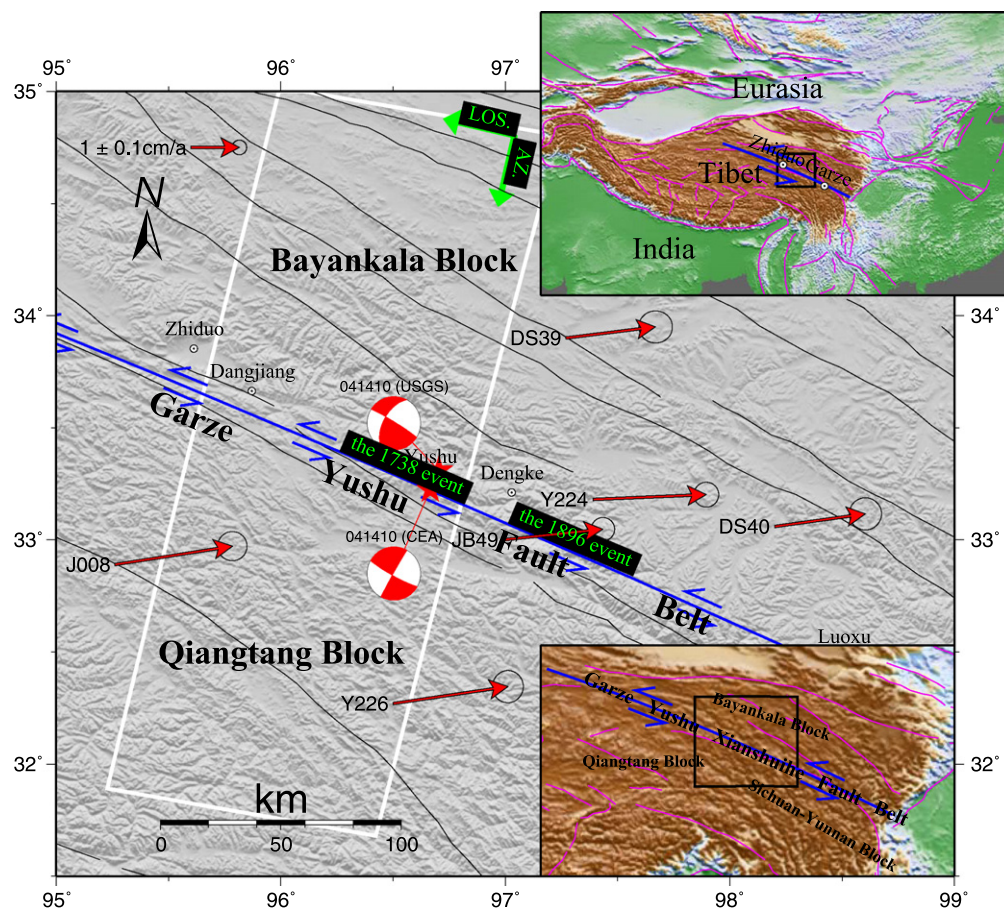


Fig. 1. Tectonic settings of the Garze–Yushu Fault belt, which is located in the center of the Tibetan Plateau, strikes northwest, with a length of about 500 km. White rectangle delimits the extents of the InSAR data (Track 276). Thin black lines denote the Quaternary active faults (Deng et al., 2003). The red arrows are GPS velocities in a Eurasia-fixed reference frame (Gan et al., 2007) being used in Fig. 5 (without Y224). On April 14, 2010, an Mw 6.9 earthquake occurred here, and two earthquake source mechanism (from CEA and USGS, respectively) are plotted. Inset maps show the interest area in this study with the major tectonic faults (Peltzer and Saucier, 1996).

for contemporary slip rates along Garze–Yushu fault, and the value ranges from 3.1 mm/yr for the NW segment (where the Yushu fault is located) to 13.0 mm/yr for the SE segment. Using GPS data and an elastic block model, Wang et al. (2011) estimated the slip rate along the Xianshuihe fault which also includes the Yushu part studied in this paper is up to 18.2 mm/yr. Large discrepancy among results derived from GPS and geological data exists, and the reason for this can be mainly attributed to different types of observations with timescales differing by a factor of a thousand at least, or to different datasets even with the same type of observations, and then other independent measuring data are further needed to evaluate the slip rate.

In this research, we examine 20 scenes of Envisat ASAR images (descending track: 276; period: from 2003 to 2010) covering the Yushu segment of the Garze–Yushu fault belt to measure the interseismic surface deformation field using InSAR time series technology. We estimate the interseismic slip rate with different locking depths, different dip angles and different rake angles, using a buried planar dislocation in an elastic half space (Okada, 1992). We then plot a lookup figure to investigate the relationships among the rake angle, the dip angle, the locking depth and the slip rate, and obtain the optimal slip rate together with other independent data. Finally, we investigate the earthquake recurrence interval and strain release along the Yushu part of Garze–Yushu fault.

2. Data and methods

2.1. Data

During the period from the launch of the Envisat satellite in 2002 to the Yushu Mw 6.9 earthquake of April 14, 2010, there were two descending tracks (Tracks 4 and 276) and two ascending tracks (Tracks 455 and 498) which imaged the Yushu part of the Garze–Yushu Fault zone. The limited SAR data and/or their poor perpendicular baselines from Tracks 4, 455 and 498, make them not good datasets to obtain a high-precision InSAR displacement field, especially when measuring the minor interseismic deformation. Fortunately, 20 images of Track 276 can be used to extract reliable deformation with InSAR time series technique.

All interferograms with perpendicular baselines less than 100 m are produced from the ASAR raw images using the Caltech/JPL ROI_PAC software (Rosen et al., 2004). The 3 arc-second Shuttle Radar Topography Mission (SRTM) Digital Elevation Model (DEM) dataset is used to remove the topographic phase component (Farr et al., 2007), and the Statistical-cost network-flow algorithm for phase unwrapping (SNAPHU) software is used to unwrap all differential interferograms (Chen and Zebker, 2002). All 63 interferograms are finally geocoded to the geographic coordinate system.

The geocoded interferograms often have unwrapping errors which appear as 2π phase jumps which can be

distinguished easily once plotted. To remove this phenomenon as far as possible, the phase closure technique developed by Biggs and her colleagues is used to identify and correct the remaining unwrapping errors (Biggs et al., 2007). Further, we only select the interferograms which have observations on both sides of the fault trace, resulting in 18 interferograms being excluded. Finally, to increase the Signal-to-Noise Ratio (SNR) of the interferograms, only those 11 interferograms with temporal baselines larger than 1 yr are used in the following InSAR time series (Fig. 2).

2.2. Methods

InSAR time series techniques are an effective method to reduce the atmospheric effects, orbital ramps, and other un-modeled errors on radar measurements (Li et al., 2009; Schmidt and Bürgmann, 2003; Wei et al., 2010). In particular, using InSAR to measure interseismic surface deformation, Biggs et al. (2007) proposed a multi-interferogram InSAR time series method, which uses an iterative algorithm with four key steps: correction of orbital errors, correction of atmospheric turbulent errors, construction of a rate map and estimation of the fault slip rate. Elliott et al. (2008) improved Biggs et al. (2007) method by correcting the atmospheric signal correlated with topography and used it to estimate the slip rate along the Altyn Tagh fault, northern Tibet. Wang et al. (2009) made use of the method from Elliott et al. (2008) to construct the LOS deformation on the northwestern Xianshuihe fault with ERS-1/2 and Envisat data, to further assess its interseismic slip rate.

Consistent with these previous methods (Biggs et al., 2007; Elliott et al., 2008; Wang et al., 2009), the method used in this research is as follows with Fig. 3 showing the corresponding flow chart:

- (a) Based on the previous geophysical, geological, and GPS results, we propose the fault geometry, including strike, dip angle, rake angle and locking depth, and the slip rate (for the first-time run, let slip rate equal to a given value; for the latter iterations, slip rate equals to the estimated value from the last iteration). We then compute the forward interseismic deformation field according to the dislocation formulas in an elastic half space (Okada, 1992) and remove this a priori deformation interferogram by interferogram.
- (b) A planar ramp is removed to minimize the orbit and other long wavelength errors, then phase-topography correlation of each interferogram is estimated and used to remove atmospheric signals correlated with topography.
- (c) To refine interferograms further, phase resulting from turbulent processes in the atmosphere for each interferogram is estimated by high-pass filtering along the time axis and low-pass filtering to across each SAR coverage, and then removed interferogram by interferogram.

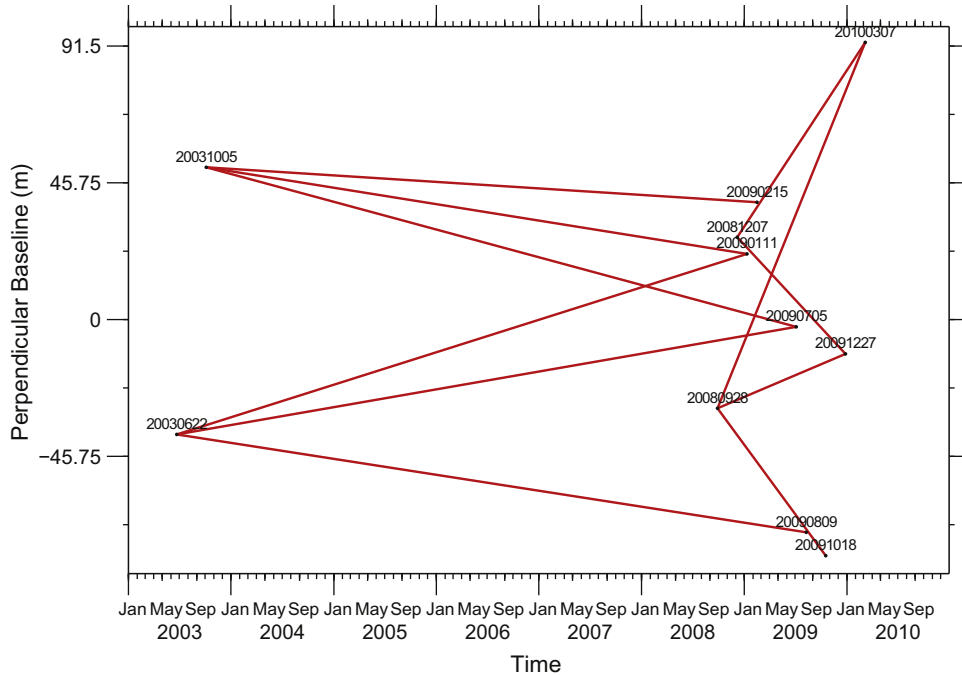


Fig. 2. Spatial and temporal baselines for Track 276. Red lines show image interferometric pairs to be processed using InSAR time series method.

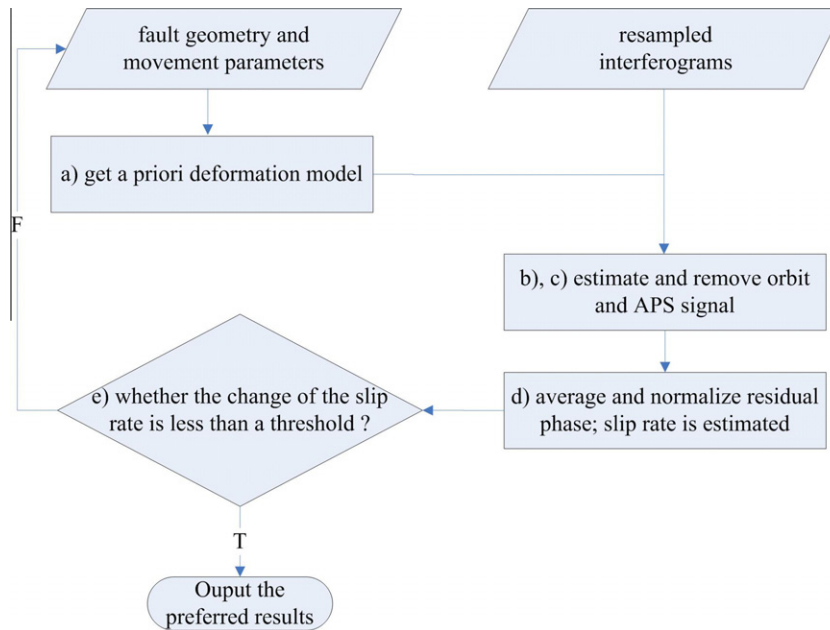


Fig. 3. Flow chart for the InSAR time series method.

- (d) The residual phase of the interferograms is averaged and normalized, and is superimposed with the priori deformation model. Finally, a slip rate is estimated by linear least squares.
- (e) Return to step (a) until the variation of the estimated slip rate is less than a threshold, such as 0.01.

During processing, we repeat the InSAR time series analysis each time we change the rake angle, the dip angle, or the locking depth and estimate the slip rate simultaneously. Then, based on all these parameters (rake angles, dip angles, and locking depth) and results (slip rates), we plot a figure which shows the relations among these four variables

(Section 3.2), which can be used as a lookup figure to find the parameters to be determined, jointly using the other independent information about the fault being studied.

3. InSAR deformation map and slip rate inversion

3.1. InSAR LOS deformation map

An interseismic rate map (Fig. 4) is derived by estimation of a constant rate on each pixel by least squares, weighing all points equally, where each pixel being coherent throughout the data set is not required (Biggs et al., 2007). Due to the good coherences in the southern part of the Garze–Yushu fault, its southern side has more observations than the northern side. Assuming that the signal in Fig. 4 is dominated by the aseismic surface motion, a steep displacement gradient across the fault trace can be easily observed. Supposing that the motion is predominately horizontal and parallel to a local strike of the Garze–Yushu fault, the deformation pattern is consistent with left-lateral shear movement.

The InSAR LOS deformation map also shows some exceptional signals, such as in the extreme northern part

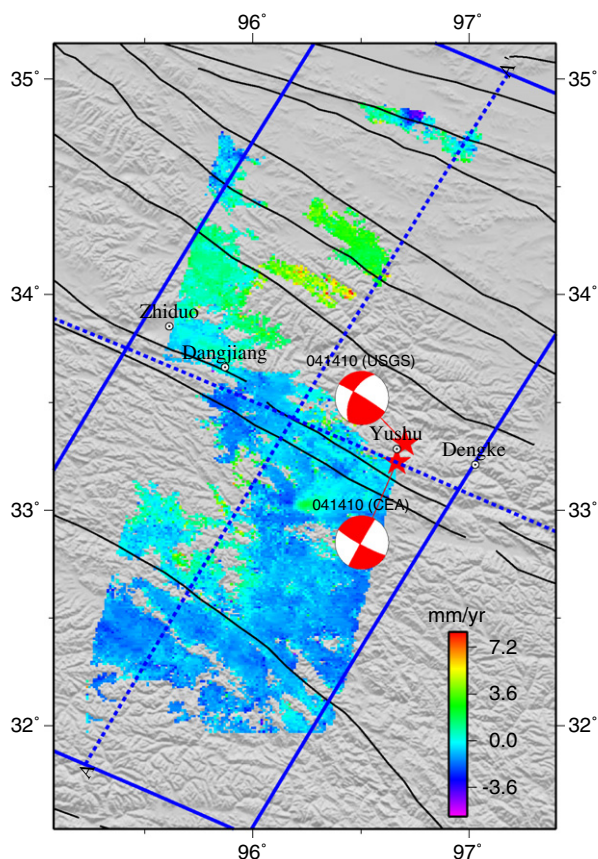


Fig. 4. LOS rate map derived from 11 interferograms after removing orbital and atmospheric delay phases. Positive values (red) are for areas of movement away from satellite, and negative values (green) for areas of movement approaching to satellite. Pixels located in the blue rectangle are plotted in Fig. 5. Thin black lines denote the Quaternary active faults.

and in the left center of the southern part. However, this signal is not well resolved and might be affected by the remaining topography-dependent atmospheric effects.

To illustrate the LOS rate map more clearly, we extract a swath profile across the InSAR rate map (Fig. 4) and show it in Fig. 5. From both the scatter plot (blue dots)¹ and mean value plot (black lines with error bar) of the Fig. 5, we can observe an approximate arctangent sigmoid curve across the fault trace (gray vertical bar), which shows that the observed velocity increases with distance from the fault. The general trend of the LOS profile is consistent with the theoretical model (red curve in Fig. 5), where the assumed fault has a vertical fault plane and strikes with only left-lateral motion, and the locking depth and slip rate are 15 km and 6.4 mm/yr, respectively. Five GPS data (purple lines with error bar) are also projected into InSAR LOS direction, which shows good consistent with both InSAR observations and theoretical model.

Close to the near-field zone (around the geological fault trace), the consistency between the observed and model profiles is slightly worse. The possible reason for it is the fact that a single fault model is used in this study, without attention to details of the fault geometry and movement, which we will take into account in the future by segmenting the fault into several parts and estimating the corresponding parameters, respectively. However, we need to specify that the theoretical arctangent curve falls into the range of the mean value plot when considering one-time standard deviation (Fig. 5).

3.2. Slip rate inversion

The InSAR deformation map across the fault can be well explained by a buried planar dislocation in which the fault is driven from a freely slipping fault at depth embedded in a homogeneous, elastic half space (Wang et al., 2009). At the same time, it is also common knowledge that most studies using GPS use the same model (Bürgmann et al., 2006; Feigl et al., 1993; Gan et al., 2007). For example, Gan et al. (2007) modeled the GPS deformation of the northeastern plateau by deep slip of simple dislocation segments locked 20 km to the surface and slipping below to an infinite depth in an elastic half space (Okada, 1992), and determined the slip rate for each dislocation by minimizing the Root Mean Square (RMS) velocity of all the GPS observations around the area. During the processing of the InSAR time series, we use a buried elastic dislocation model in an elastic half space (Okada, 1992) to remove and restore the aseismic surface deformation relative to the deep fault slip movement.

As we know, the locking depth and deep slip rate are significantly correlated with each other when both are estimated simultaneously using geodetic data (Fialko, 2006;

¹ For interpretation of color in Figs. 1–8, the reader is referred to the web version of this article.

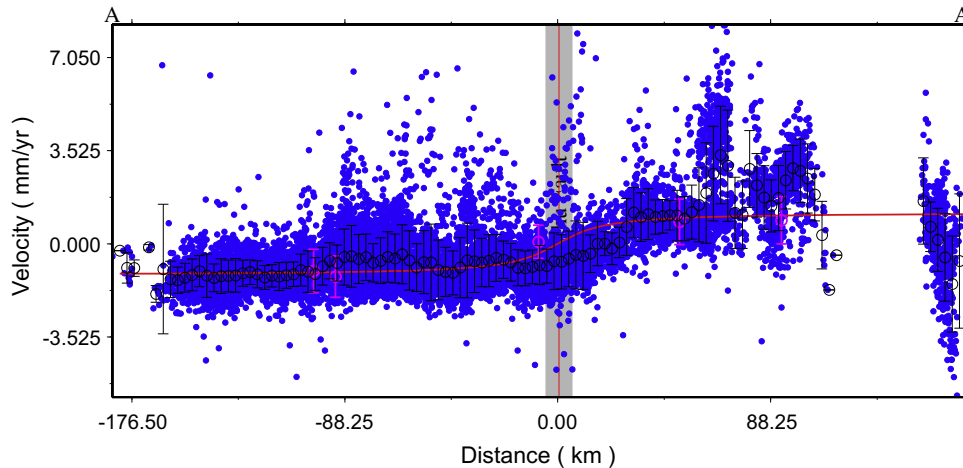


Fig. 5. Profile across InSAR LOS rate map (Fig. 4). LOS rate (Vertical Axis) is plotted according to distance (Horizontal Axis) from the fault. Each pixel is represented by a single dot on the scatter plot. Black error bars denote the one-time standard deviation of the point measurements within the 3-km-wide bin along the profile. Purple error bars denote 5 GPS data (Fig. 1) projected into InSAR LOS direction. The red line represents the theoretical LOS displacement, where the assumed fault has a vertical fault plane and strikes with only left-lateral motion, and the locking depth, slip rate are 15 km, 6.4 mm/yr, respectively.

Segall, 2002). When increasing the locking depth, the slip rate needs to have a higher value to achieve the same surface deformation. Also, to a certain degree, there is a trade-off between the dip and the slip rate (Bendick et al., 2000).

In this research, unlike the previous research, we estimate the interseismic slip rate with different locking depths, different dip angles and different rake angles, using a buried planar dislocation in an elastic half space (Okada, 1992). Then, we plot a lookup figure to investigate the relationships among the rake angle, the dip angle, the locking depth and the slip rate. The process can be illustrated, for example, as:

We assume that the rake angle of the modeled fault equals -10° , the dip angle is 74° , the locking depth is 3 km, and the slip rate is assigned a nominal value (e.g., 1); we then do the InSAR time series as demonstrated by Section 2.2, and the slip rate can be determined when iteration outcomes converge.

For the computations in this process, a slip rate is estimated each time we change the rake angle from -10° to 10° by a step of 2° , the dip angle from 74° to 90° by a step of 2° , the locking depth from 3 km to 21 km by a step of 2 km, successively. So, 990 ($11 * 9 * 10$) analyses of InSAR time series on the slip rate are done, and then a figure showing the relationships among the rake angle, the dip angle, the locking depth and the slip rate is plotted as in Fig. 6. Correspondingly, Fig. 7 shows the RMS misfits for each fault geometry model, all of which are slightly higher than 1 mm, suggesting a good fit to the observations.

From Fig. 6, we find out that the estimated slip rate changes a lot when the locking depth varies from 3 km to 21 km, and also changes significantly when rake angle ranges from -10° to 10° , but only changes a little when the dip angle varies from 74° to 90° , regardless of the

magnitude of the locking depth. The estimated slip rate changes from ~ 2.6 mm/yr to ~ 21.1 mm/yr, when the locking depth ranges from 3 km to 21 km.

According to Fig. 7, the locking depth seems to have a higher value than 15 km, model of which can achieve a lower RMS misfit (1.02 mm) of the observations. This depth is almost consistent with the coseismic rupture depth of the 2010 April 14 Mw 6.9 Yushu earthquake (Li et al., in press; Liu et al., 2010; Zhang et al., 2010), which may suggest that the 2010 event almost ruptured through all the locking depth.

4. Discussion

4.1. Determination of dip angle, rake angle and locking depth

From Section 3.2, we know that the estimated slip rate hardly changes with the dip angle, regardless of the magnitude of the locking depth. The reason for this can be mainly attributed to the low sensitivity of surface deformation to the dip angle of the deep dislocation model. In addition, if the rake angle is fixed and only the dip angle varies, then the pattern of the surface deformation from the deep dislocation model may not change significantly, but it changes from symmetric to asymmetric.

When the dip angle varies from 74° to 90° , the global deformation pattern remains the same. During the InSAR time series process, while a planar ramp is removed to reduce orbit ramps and other long wavelength errors, the effect due to the variable dip is also minimized. Therefore, we conclude that using images from one track (descending or ascending) may not constrain the dip angle well.

Regardless of the magnitude of the locking depth, when the rake angle changes, the estimated slip rate also changes. The reason for this can be mainly attributed to the high

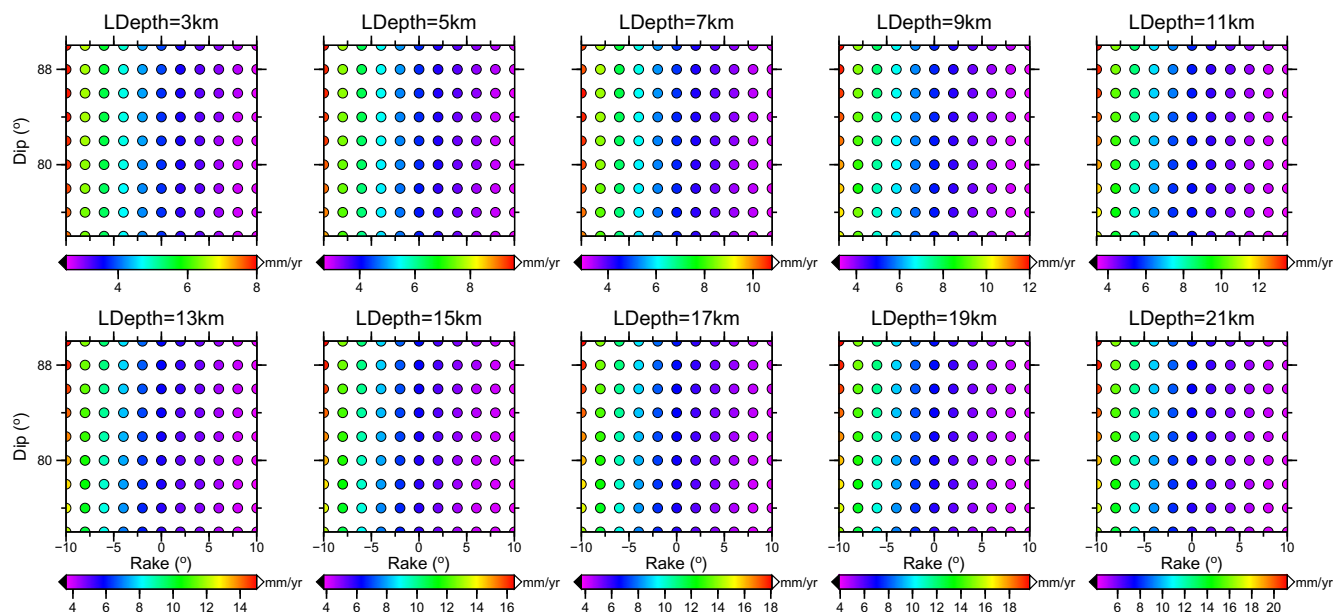


Fig. 6. Slip rate map from inversion of InSAR data only for different locking depths, different rake angles and different dip angles. A slip rate is estimated each time we change the rake angle from -10° to 10° by a step of 2° , the dip angle from 74° to 90° by a step of 2° , and the locking depth from 3 km to 21 km by a step of 2 km, successively.

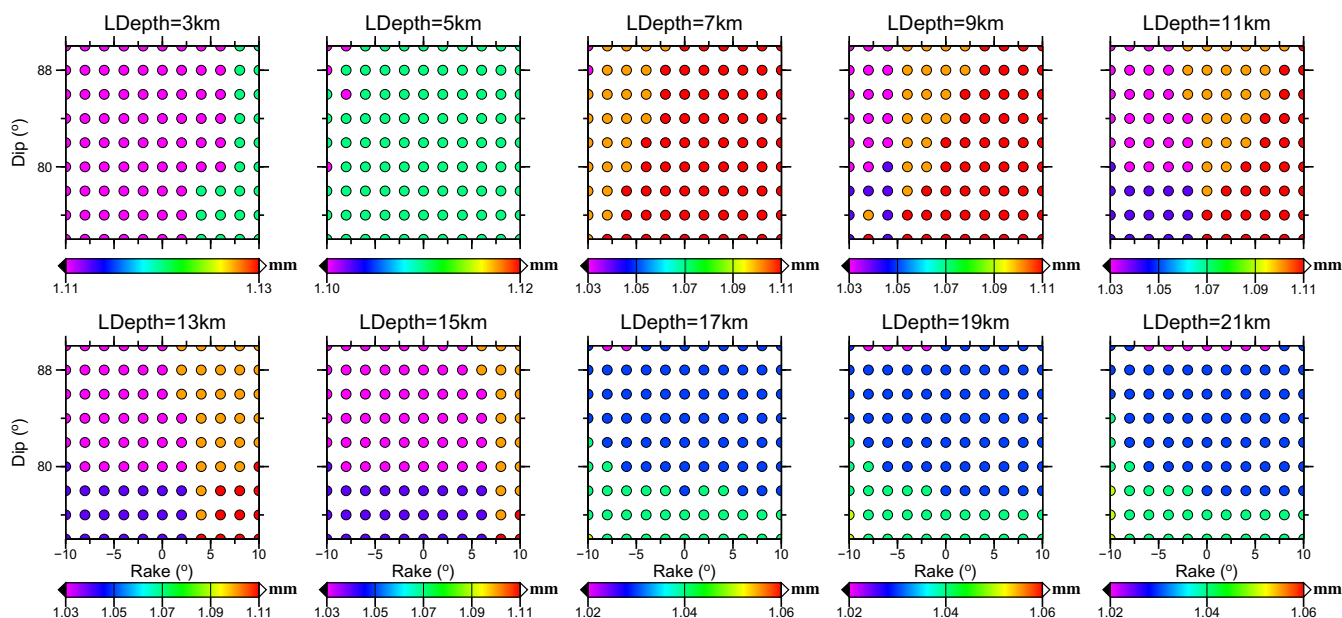


Fig. 7. RMS misfits of the observations for each fault geometry model in Fig. 6.

sensitivity of surface deformation to the rake angle of the deep dislocation model. If the dip angle is constant and only the rake angle varies, then the pattern of the surface deformation from the deep dislocation model may change. At the same time, it is also related to the fact that the InSAR data are only one component data (in the LOS direction). Thus the estimated slip rate is strongly dependent on the assumed projection of the slip into the LOS direction, which depends on the rake angle. Then, if data about the locking depth and slip rate can be provided

accurately, by referring to Fig. 6 the rake angle and the corresponding confidence interval can be determined, properly.

For the locking depth, the estimated slip rate also changes with it. For example, when the rake angle equals 0° and dip angle 90° , the estimated slip rate increases from ~ 3.9 mm/yr to ~ 7.7 mm/yr as the locking depth increases from 3 km to 21 km, which is consistent with the fact that the slip rate needs to a higher value to achieve the same surface deformation while increasing the locking depth

(Segall, 2002). In this case, as with the method of the rake angle estimation mentioned in the preceding paragraph, we can obtain a reasonable estimate for the locking depth once we determine the slip rate and rake angle from other independent data.

4.2. Determination of slip rate

Segall (2002) used a bootstrap resampling procedure to determine the range of slip rate and locking depth. Segall's results show that the slip rates on the San Andreas Fault system in the range of 34–41 mm/yr are consistent with GPS observations. In this research, a lookup figure (Fig. 6) is made to show the relationships among the rake angle, the dip angle, the locking depth and the slip rate (Section 3.2), which can be used to find the preferred slip rate. Fig. 6 shows the possible slip rates when a priori knowledge of the Garze–Yushu fault geometry is known. Thus, a combination of multi-disciplinary knowledge is required to quantify the slip rate of the Garze–Yushu fault.

The April 14, 2010 Yushu Mw 6.9 earthquake (33.2°N, 96.6°E), with a focal depth of 14 km and a rake angle of -2° (Li et al., in press; Liu et al., 2010; Zhang et al., 2010), occurred on the Garze–Yushu fault belt which is located in the center of the Tibetan Plateau (Fig. 1). This earthquake created three left-stepping fault ruptures: the northern primary rupture with a length of about 16 km; the central one with a length of about 9 km; and the southern one with a length of about 7 km (Chen et al., 2010). Additionally, two large earthquakes have been officially recorded over the last 200 yr, including the December 23, 1738 Mw 6.5 earthquake occurred in and to the northwest of Yushu, Qinghai Province, and the March 1896 M 7.0 earthquake occurred between Luoxu, Shiqu county, Sichuan Province and Yushu, Qinghai Province (Group of the Data Compilation of Earthquakes in Sichuan, 1980). What is more, the fact that the epicenter of the December 23, 1738 Qinghai Yushu earthquake revealed by the isoseismal map (Institute of Geophysics, China Earthquake Administration, 1990) has almost the same place with the seismogenic segment of the April 14, 2010 Mw 6.9 earthquake, indicates an in situ recurrence of large earthquakes (Chen et al., 2010).

According to these historical earthquake records, we can assume that the locking depth for Yushu part of the Garze–Yushu fault belt equals 15 km, the rake angle is about 0° , and we can conclude that the interseismic slip rate for the Yushu part of the Garze–Yushu fault is close to a value of 6.4 mm/yr after consulting Fig. 6. As suggested by Section 4.1, the slip rate does not correlate with the dip angle, obviously, so we do not consider the effect on the slip rate estimation of the dip angle.

4.3. Joint inversion of GPS and InSAR data

It is common knowledge that there is a strong tradeoff between slip rate and locking depth using the InSAR data alone, caused in large part by a correlation between the

long-wavelength ramp of InSAR and the sigmoidal pattern of interseismic deformation. Addition of GPS data to InSAR data can help to resolve this problem (Wang et al., 2009).

As shown in Fig. 1, a total of 6 GPS stations are near the observation extent of InSAR and the Garze–Yushu fault belt, and only 1 GPS station (Y226) is located within the observation extent of InSAR. Additionally, due to having different fault-parallel velocity characteristics from the other 5 GPS stations, station Y224 is not used to combine with InSAR data to evaluate slip rate. Joint inversion of GPS and InSAR data shows that the estimated slip rate ranges from ~ 3.0 mm/yr to ~ 14.2 mm/yr (Fig. 8), range of which is narrower than that (from ~ 2.6 mm/yr to ~ 21.1 mm/yr) derived from inversion of InSAR data only, when the locking depth ranges from 3 km to 21 km. This is similar to the conclusions of Wang et al. (2009) who found that the range of slip rate is reduced evidently with the joint inversion of GPS and InSAR data. Still assuming the same priori information of locking depth and rake angle as that in Section 4.2, the preferred slip rate of the Garze–Yushu fault is close to a value of 6.0 mm/yr, which is fairly close to the 6.4 mm/yr derived from inversion of InSAR data only.

Due to not enough common space coverage between GPS and InSAR data and possible different slip rate for different parts of the Garze–Yushu fault, we adopt slip rate results from inversion of InSAR data only in the following sections, although joint inversion of GPS and InSAR data can provide a narrower range of slip rate.

4.4. Comparison with other slip results

Previous geological studies have suggested that the Quaternary strike-slip rate of the Garze–Yushu fault belt ranges from ~ 7 mm/yr to 14 mm/yr (Wang et al., 2008a; Wen et al., 2003; Zhou et al., 1996). Based on the regional geological mapping results and interpretation of satellite images and aerial photos in combination with detailed field investigations, Zhou et al. (1996) generated a spatial distribution of the recent surface activity of the Garze–Yushu fault belt. Furthermore, the faulted landform, deformation and displacement of young deposit layers, and results of geologic chronology (Carbon 14 and Thermoluminescence dating) suggested that the fault horizontal average slip rate of the Yushu part of the Garze–Yushu fault belt since later Quaternary is about 7 mm/yr. Wen et al. (2003) re-investigated the later Quaternary activity and recent large earthquake ruptures of the Garze–Yushu fault, and determined that the average left-lateral slip rate along the fault is about 12 mm/yr for the last 50,000 yr from both offset landforms and ages of the correlative sediments at 7 locations. Wang et al. (2008a) documented the distribution of stream deflections along the Garze–Yushu segment of the Xianshuihe fault, and proposed that the Holocene slip rate decreased from 10 to 14 mm/yr around Dengke (SE) to about 7 mm/yr around Dangjiang (NW), and the Yushu

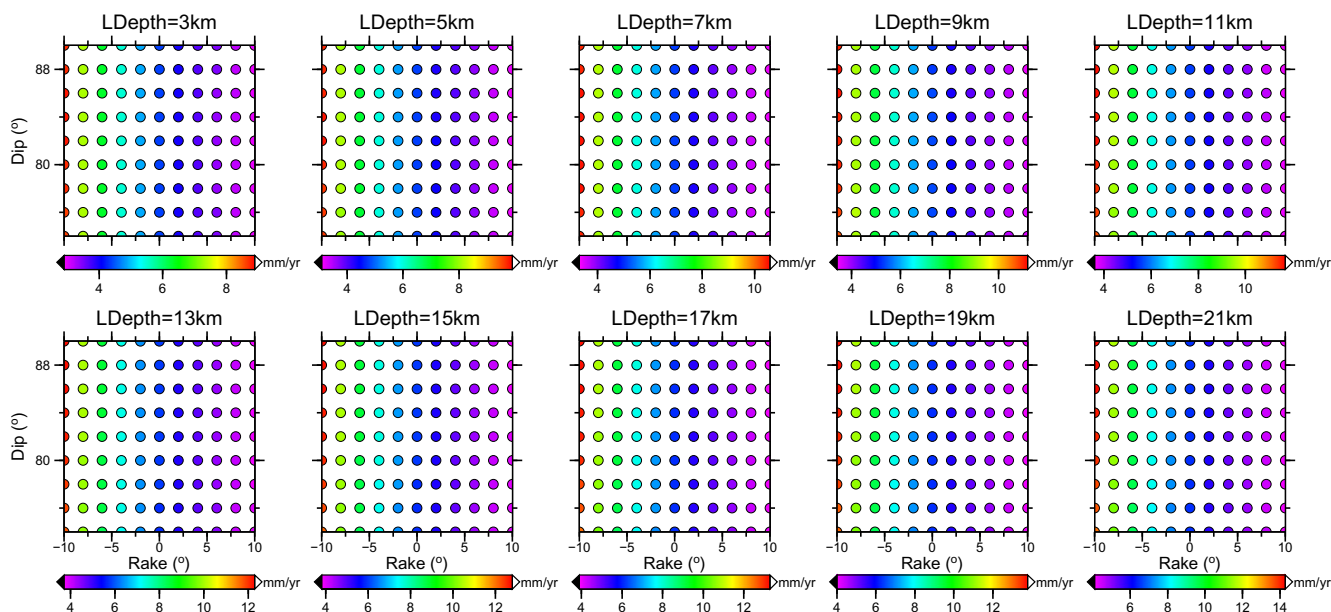


Fig. 8. Same as Fig. 6 but here slip rate map is derived from joint inversion of GPS and InSAR data.

segment studied in this paper is located between these two sites geographically.

The GPS velocity field across the Garze–Yushu fault belt indicates that the decennial-scale strike-slip rate of the fault belt is around 10 mm/yr (Gan et al., 2007; Meade, 2007; Wang et al., 2008b, 2011), but there exist large discrepancies among results derived from different papers.

In this research, the preferred slip rate approximates to a value of 6.4 mm/yr, falling between the highest (18.2 mm/yr) and the lowest (3.1 mm/yr) slip rates from GPS estimations (Gan et al., 2007; Meade, 2007; Wang et al., 2008b, 2011), but less than the minimum value (~ 7 mm/yr) from the geological estimations (Wang et al., 2008a; Wen et al., 2003; Zhou et al., 1996). The reason for this outcome can be attributed to different types of InSAR data from GPS and geological data, or to the complexity of the fault geometry and movements which have been determined by geological and remote sensing results (Wang et al., 2008a; Wen et al., 2003; Zhou et al., 1996) which show that not only strike slip movement but also transtensional and transpressional structures such as pullapart basins and thrust faults along different parts of the fault at different times can accommodate the tectonic evolution of the central eastern Tibet.

These slip rate discrepancies can be reduced if we modify the former assumed locking depth and rake angle. From Fig. 6, if we assumed that the locking depth equals to a value of 21 km from one or more external data set(s), then the estimated slip rate would range from ~ 4.2 mm/yr to ~ 21.1 mm/yr, depending on the rake angle. Additionally, if we assumed that the locking depth equals 3 km from one or more external data set(s), then the estimated slip rate would range from ~ 2.6 mm/yr to ~ 7.9 mm/yr, also depending on the rake angle. So, to quantify quite a

narrow range of the slip rate, more independent data sets are requested to provide more prior information about the fault locking depth, rake angle, and so on.

4.5. Earthquake recurrence interval and strain release

After the April 14, 2010 Mw 6.9 earthquake, Chen et al. (2010) acquired the images of the earthquake surface rupture by rapid and exhaustive field investigations, and compared it with large historical earthquake on the Garze–Yushu fault, showed that the Garze–Yushu fault dominated the occurrence of the April 14, 2010 Mw 6.9 Yushu earthquake, and had short-term recurrence intervals of large earthquakes ranging from 274 yr to 677 yr, with 274 yr for the Yushu part where the 2010 earthquake happened.

If the April 14, 2010 Mw 6.9 earthquake and the December 23, 1738 Mw 6.5 earthquake are considered as a couple of characteristic earthquakes along the Yushu part of the Garze–Yushu fault, the recurrence interval for this part can be considered to be about 272 yr, in good agreement with the recurrence interval of 274 yr from Chen et al. (2010). Given this recurrence interval, knowing the average slip rate for this part allows us to make an estimate of the accumulated slip deficit of this part by multiplying the recurrence interval (272 yr) and the average slip rate (6.4 mm/yr). As a result, the Yushu part of the Garze–Yushu fault accumulated a slip deficit of about 1.74 m between December 23, 1738 and April 14, 2010.

According to the coseismic surface rupture data from Chen et al. (2010), the measured horizontal strike slip displacement of the northern primary rupture is between 1.1 m and 1.8 m, the maximum measured horizontal displacement of the central one is 0.9 m, and the measured

horizontal displacement of the southern one at 32°57'19.7"N, 97°02'01.3"E is 0.5 m. On the whole, a good consistency between the interseismic accumulated slip deficit and the coseismic surface rupture can be found. The discrepancy between them can be attributed either to the errors in estimating the slip rate due to the InSAR deformation errors or the simplified fault model, or to the possible man-made errors in estimating surface ruptures in the field, or to the possibility that the 2010 event only released part of the accumulated strain energy, or to near-surface effects due to the inelastic seismic response of the brittle uppermost crust (e.g., Fialko et al., 2005; Xu et al., 2010).

Assuming that the formula $M_0 = \mu W L s$ is available to compute the scalar seismic moment (M_0), where μ is the elastic shear modulus (3.2×10^{10} Pa), W the fault width (15 km), L the fault rupture length, and s the average slip on the fault, knowing the fault rupture length (L) and seismic moment (M_0) allows us to estimate the average slip (s) on the fault. GCMT moment tensor solutions show that the released seismic moment of the April 14, 2010 Yushu earthquake is 2.5×10^{19} Nm (USGS, 2010). If the rupture length is fixed as 31 km (Chen et al., 2010), an estimate for the average slip of 1.68 m on the fault is obtained, very close to the accumulated slip deficit of about 1.74 m, indicating that the April 14, 2010 Mw 6.9 Yushu earthquake has released almost all the accumulated strain energy. If we take the en-echelon tensile fissure zone with a length of 2 km as the north end of the rupture zone, the rupture would have a length of about 51 km (Chen et al., 2010; Li et al., in press), then the estimated average slip is about 1.02 m, which is less than the accumulated slip deficit of about 1.74 m, indicating that the April 14, 2010 Mw 6.9 Yushu earthquake has not released the accumulated strain energy between 1738 and 2010 completely, and that the Yushu part with 0.72 m of slip deficit still suffer a seismic risk in the future.

5. Conclusions

In this paper, we estimate the interseismic surface deformation along the Yushu part of the Garze–Yuhai fault using InSAR time series technology based on the Envisat ASAR data (descending track: 276) between 2003 and 2010. We conduct 990 ($11 * 9 * 10$) analyses of InSAR time series on the slip rate for different rake angles, different dip angles, and different locking depths, and plot a lookup figure to investigate the relationships among the rake angle, the dip angle, the locking depth and the slip rate, from which we can determine the preferred estimate, and the corresponding error band if the error ranges of the independent data can be given quantitatively.

A combination of multi-disciplinary knowledge is required to quantify the slip rate of the Garze–Yuhai fault. When considering the focal mechanism solutions of the historical earthquake records along this fault belt, the interseismic slip rate for the Yushu part of the Garze–Yuhai fault

is close to a value of 6.4 mm/yr. There exist slip rate discrepancies among the estimations derived from InSAR, GPS and geological observations, and the reasons for this can be attributed three aspects. First InSAR data is a different type of observation from GPS and geological data, second we only use an ideal single fault model whereas the fault geometry and movement is very complex indeed, and third the prior information about the fault locking depth and rake angle are not sufficient to constrain the fault properties accurately. When the April 14, 2010 Mw 6.9 earthquake has a rupture length of 51 km, the slip rate equals 6.4 mm/yr, and the earthquake recurrence interval on the Yushu part of Garze–Yuhai fault equals 272 yr, the April 14, 2010 Mw 6.9 earthquake has not released all the accumulated strain energy between 1738 and 2010, and the Yushu part with 0.72 m of slip deficit still suffer a seismic risk in the future.

At the same time, our results show that using images from one track (descending or ascending) may not constrain the dip angle well, and both the ascending and descending observations shall be used to optimize the slip rate inversion in the future.

Acknowledgments

This work was supported by the National Natural Science Foundation of China (No. 41074007, 40974017, 41021061, and 40874003), the 111 Project and the National Department Public Benefit Research Foundation (Earthquake) (No. 200808080), the National High Technology Research and Development Program of China (863 Program) (No. 2009AA12Z317), the Specialized Research Fund for the Doctoral Program of Higher Education (No. 20090141110055), the Fundamental Research Funds for the Central Universities (No. 3101036), and the Open Research Fund Program of the Key Laboratory of Geospace Environment and Geodesy (LOGEG), Ministry of Education, China (No. 10-02-11). Part of this work was carried out in the University of Glasgow, which was supported by the Natural Environmental Research Council (NERC) through the GAS project (Ref: NE/H001085/1). The ASAR data were supplied by ESA through the ESA-NRSCC DRAGON2 project (ID: 5343). Most figures were made using Generic Mapping Tools version 4.5.1. We thank Jeffrey Freymueller, one anonymous reviewer, and Editor Jan Las-tovicka for comments that improved the manuscript.

References

- Bendick, R., Bilham, R., Freymueller, J., Larson, K., Yin, G. Geodetic evidence for a low slip rate in the Altyn Tagh fault system. *Nature* 404 (6773), 69–72, 2000.
- Biggs, J., Wright, T., Lu, Z., Parsons, B. Multi-interferogram method for measuring interseismic deformation: Denali Fault, Alaska. *Geophys. J. Int.* 170 (3), 1165–1179, doi:10.1111/j.1365-246X.2007.03415.x, 2007.
- Bock, Y., Prawirodirdjo, L., Melbourne, T.I. Detection of arbitrarily large dynamic ground motions with a dense high-rate GPS network. *Geophys. Res. Lett.* 31, L06604, doi:10.1029/2003GL019150, 2004.

- Bürgmann, R., Hilley, G., Ferretti, A., Novali, F. Resolving vertical tectonics in the San Francisco Bay Area from permanent scatterer InSAR and GPS analysis. *Geology* 34 (3), 221–224, doi:10.1130/G22064.1, 2006.
- Cavalié, O., Lasserre, C., Doin, M.P., Peltzer, G., Sun, J., Xu, X., Shen, Z.K. Measurement of interseismic strain across the Haiyuan fault (Gansu, China), by InSAR. *Earth Planet. Sci. Lett.* 275 (3–4), 246–257, 2008.
- Chen, C.W., Zebker, H.A. Phase unwrapping for large SAR interferograms: statistical segmentation and generalized network models. *IEEE Trans. Geosci. Remote Sensing* 40 (8), 1709–1719, 2002.
- Chen, L.C., Wang, H., Ran, Y.K., Sun, X.Z., Su, G.W., Wang, J., Tan, X.B., Li, Z.M., Zhang, X.Q. The M_s 7.1 Yushu earthquake surface rupture and large historical earthquakes on the Garzê–Yushu Fault. *Chinese Sci. Bull.* 55 (31), 3504–3509, 2010.
- Deng, Q.D., Zhang, P.Z., Ran, Y.K., Yang, X.P., Min, W., Chu, Q.Z. Basic characteristics of active tectonics of China. *Sci. China Ser. D* 46 (4), 356–372, 2003.
- Elliott, J.R., Biggs, J., Parsons, B., Wright, T.J. InSAR slip rate determination on the Altyn Tagh Fault, northern Tibet, in the presence of topographically correlated atmospheric delays. *Geophys. Res. Lett.* (L12309), 35, doi:10.1029/2008gl033659, 2008.
- Farr, T.G., Rosen, P.A., Caro, E., Crippen, R., Duren, R., Hensley, S., Kobrick, M., Paller, M., Rodriguez, E., Roth, L. The shuttle radar topography mission. *Rev. Geophys.* (2), 45, doi:10.1029/2005RG000183, 2007.
- Feigl, K.L., Agnew, D.C., Bock, Y., Dong, D., Donnellan, A., Hager, B.H., Herring, T.A., Jackson, D.D., Jordan, T.H., King, R.W. Space geodetic measurement of crustal deformation in central and southern California, 1984–1992. *J. Geophys. Res.* 98 (B12), 21677–21712, 1993.
- Fialko, Y., Sandwell, D., Simons, M., Rosen, P. Three-dimensional deformation caused by the Bam, Iran, earthquake and the origin of shallow slip deficit. *Nature* 435 (7040), 295–299, 2005.
- Fialko, Y. Interseismic strain accumulation and the earthquake potential on the southern San Andreas fault system. *Nature* 441 (7096), 968–971, 2006.
- Gan, W., Zhang, P., Shen, Z.-K., Niu, Z., Wang, M., Wan, Y., Zhou, D., Cheng, J. Present-day crustal motion within the Tibetan Plateau inferred from GPS measurements. *J. Geophys. Res.* (B08416), 112, doi:10.1029/2005jb004120, 2007.
- Gourmelen, N., Amelung, F., Lanari, R. Interferometric synthetic aperture radar–GPS integration: interseismic strain accumulation across the Hunter Mountain fault in the eastern California shear zone. *J. Geophys. Res.* (B9), 115, doi:10.1029/2009jb007064, 2010.
- Group of the Data Compilation of Earthquakes in Sichuan. A data Compilation for Earthquakes in Sichuan (Book 1). Sichuan People's Publishing House, Chengdu, 1980 (In Chinese).
- Hanssen, R.F. *Radar Interferometry: Data Interpretation and Error Analysis*. Kluwer Acad., Dordrecht, Netherlands, 2001.
- Institute of Geophysics, China Earthquake Administration. *The Atlas of Historic Earthquakes of China (The Qing Dynasty Period)*. China Cartographic Publishing House, Beijing, 1990 (In Chinese).
- Larson, K.M., Bodin, P., Gomberg, J. Using 1-Hz GPS data to measure deformations caused by the Denali fault earthquake. *Science* 300 (5624), 1421–1424, doi:10.1126/science.1084531, 2003.
- Li, Z., Fielding, E., Cross, P. Integration of InSAR time series analysis and water vapour correction for mapping postseismic deformation after the 2003 Bam (Iran) Earthquake. *IEEE Trans. Geosci. Remote Sensing* 47 (9), 3220–3230, 2009.
- Li, Z., Elliott, J.R., Feng, W., Jackson, J.A., Parsons, B., Walters, R.J. The 2010 M_w 6.8 Yushu (Qinghai, China) earthquake: constraints provided by InSAR and body wave seismology. *J. Geophys. Res.*, in press, doi:10.1029/2011JB008358.
- Liu, C., Xu, L.S., Chen, Y.T. Quick moment tensor solution for 14 April 2010 Yushu, Qinghai, earthquake. *Acta Seismol. Sin.* 32 (3), 366–368 (In Chinese), 2010.
- Meade, B.J. Present-day kinematics at the India-Asia collision zone. *Geology* 35 (1), 81–84, doi:10.1130/g22924a.1, 2007.
- Okada, Y. Internal deformation due to shear and tensile faults in a half-space. *Bull. Seismol. Soc. Am.* 82 (2), 1018–1040, 1992.
- Peltzer, G., Saucier, F. Present-day kinematics of Asia derived from geologic fault rates. *J. Geophys. Res.* 101 (B12), 27943–27956, 1996.
- Peng, H., Ma, X.M., Bai, J.Q., Du, D.P. Characteristics of quaternary activities of the Garzê–Yushu fault zone. *J. Geomech.* 12 (3), 295–304 (In Chinese), 2006.
- Rosen, P.A., Hensley, S., Peltzer, G., Simons, M. Updated repeat orbit interferometry package released. *Eos Trans. AGU* 85 (5), 47, 2004.
- Schmidt, D., Bürgmann, R. Time-dependent land uplift and subsidence in the Santa Clara valley, California, from a large interferometric synthetic aperture radar data set. *J. Geophys. Res.* 108 (B9), 1992–2003, 2003.
- Segall, P. Integrating geologic and geodetic estimates of slip rate on the San Andreas fault system. *Int. Geology Rev.* 44, 62–82, 2002.
- USGS. http://earthquake.usgs.gov/earthquakes/eqarchives/significant/sig_2010.php, 2010 (last accessed 24.04.11).
- Wang, H., Liu, M., Cao, J., Shen, X., Zhang, G. Slip rates and seismic moment deficits on major active faults in mainland China. *J. Geophys. Res.* (B02405), 116, doi:10.1029/2010jb007821, 2011.
- Wang, H., Wright, T.J., Biggs, J. Interseismic slip rate of the northwestern Xianshuihe fault from InSAR data. *Geophys. Res. Lett.* (L03302), 36, doi:10.1029/2008gl036560, 2009.
- Wang, S., Wang, E., Fang, X., Fu, B. Late cenozoic systematic left-lateral stream deflections along the Ganzi–Yushu fault, Xianshuihe fault system, Eastern Tibet. *Int. Geology Rev.* 50 (7), 624–635, doi:10.2747/0020-6814.50.7.624, 2008a.
- Wang, Y.Z., Wang, E.N., Shen, Z.K., Wang, M., Gan, W.J., Qiao, X.J., Meng, G.J., Li, T.M., Tao, W., Yang, Y.L. GPS-constrained inversion of present-day slip rates along major faults of the Sichuan–Yunnan region. *China Sci. China Ser. D* 51 (9), 1267–1283, doi:10.1007/s11430-008-0106-4, 2008b.
- Wei, M., Sandwell, D., Smith-Konter, B. Optimal combination of InSAR and GPS for measuring interseismic crustal deformation. *Adv. Space Res.* 46 (2), 236–249, doi:10.1016/j.asr.2010.03.013, 2010.
- Wen, X., Xu, X., Zheng, R., Xie, Y., Wan, C. Average slip-rate and recent large earthquake ruptures along the Garzê–Yushu fault. *Sci. China Ser. D* 46 (Supp.), 276–288, 2003.
- Xu, C., Liu, Y., Wen, Y., Wang, R. Coseismic slip distribution of the 2008 Mw 7.9 Wenchuan earthquake from joint inversion of GPS and InSAR data. *Bull. Seismol. Soc. Am.* 100 (5B), 2736–2749, doi:10.1785/0120090253, 2010.
- Zhang, P., Deng, Q., Zhang, G., Ma, J., Gan, W., Min, W., Mao, F., Wang, Q. Active tectonic blocks and strong earthquakes in the continent of China. *Sci. China Ser. D* 46 (Supp.), 13–24, 2003.
- Zhang, Y., Xu, L.S., Chen, Y.T. Source process of the 2010 Yushu, Qinghai, earthquake. *Sci. China Ser. D* 53 (9), 1249–1251, 2010.
- Zhou, R., Ma, S., Cai, C. Late Quaternary active features of the Ganzi–Yushu fault zone. *Earthquake Res. China* 12 (3), 250–260 (In Chinese), 1996.